Available online at www.sciencedirect.com
SCIENCE DIRECT
Journal of Magnetic Resonance 178 (2006) 174–183
JMR Journal of Magnetic Resonance
www.elsevier.com/locate/jmr

Tunable-frequency high-field electron paramagnetic resonance

J. Krzystek [a,*], S.A. Zvyagin [a,1], Andrew Ozarowski [a], S. Trofimenko [b], Joshua Telser [c]

[a] National High Magnetic Field Laboratory, Florida State University, Tallahassee, FL 32310, USA
[b] Department of Chemistry and Biochemistry, University of Delaware, Newark, DE 19716, USA
[c] Department of Biological, Chemical, and Physical Sciences, Roosevelt University, Chicago, IL 60605, USA

Received 26 July 2005; revised 21 September 2005
Available online 13 October 2005

Abstract

A tunable-frequency methodology based on backward wave oscillator sources in high-frequency and -field EPR (HFEPR) is described. This methodology is illustrated by an application to three non-Kramers transition metal ion complexes and one Kramers ion complex. The complexes are of: Ni(II) ($S = 1$) as found in dichlorobistriphenylphosphanenickel(II), Mn(III) ($S = 2$) as found in meso-otetrasulfonatoporphyrinatomanganese(III) chloride, Fe(II) ($S = 2$) as found in ferrous sulfate tetrahydrate, and Co(II) ($S = 3/2$) as found in azido(tris(3-*tert*-butylpyrazol-1-yl)hydroborate)cobalt(II). The above Ni(II) and Mn(III) complexes have been studied before by HFEPR using the multifrequency methodology based on Gunn oscillator sources, but not by the present method, while the Fe(II) and Co(II) complexes presented here have not been studied by any form of HFEPR. Highly accurate spin Hamiltonian parameters can be obtained by the experimental methodology described here, in combination with automated fitting procedures. This method is particularly successful in determining *g*-matrix parameters, which are very difficult to extract for high-spin systems from single frequency (or a very limited set of multi-frequency) HFEPR spectra, but is also able to deliver equally accurate values of the zero-field splitting tensor. The experimental methods involve either conventional magnetic field modulation or an optical modulation of the sub-THz wave beam. The relative merits of these and other experimental methods are discussed.

Keywords: EPR; ESR; HFEPR; High-frequency and -field EPR; Tunable-frequency EPR; Zero-field splitting

1. Introduction

High-frequency and -field EPR (HFEPR)[2] has become in the recent years an experimental method of choice in investigating a variety of spin systems that for different reasons cannot be adequately characterized by conventional EPR [1]. The application of HFEPR to non-Kramers (integer-spin number) paramagnetic species has been particularly compelling since many such systems cannot be characterized by EPR at conventional frequencies or magnetic fields primarily due to large zero-field splitting (zfs), often exceeding the microwave quantum energy of 0.3 cm^{-1} (X-band) or 1.2 cm^{-1} (Q-band) [2]. Typical examples of HS non-Kramers species investigated by HFEPR have been 3d transition metal ions since their zfs falls into the energy range conveniently obtainable by modern sub-THz sources. Thus, metal ions such as V(III) ($3d^2$) [3], Mn(III) and Cr(II) (both $3d^4$) [4–6], Fe(II) ($3d^6$) [7], and Ni(II) ($3d^8$) [8,9] have been recently studied using HFEPR.

The methodology of extracting spin Hamiltonian parameters from HFEPR spectra has been initially the same as in conventional EPR: simulating the spectra using an initial set of spin Hamiltonian parameters, comparing the simulations with experiment, and adjusting simulation parameters in an iterative process until a satisfactory agreement was found. If—as is often the case—the sample is polycrystalline or contained in a glass, the simulation process involves

* Corresponding author. Fax: +1 850 644 1366.
E-mail address: krzystek@fsu.edu (J. Krzystek).
[1] Present address: Hochfeld-Magnetlabor Dresden, Forschungszentrum Rossendorf, D-01328 Dresden, Germany.
[2] *Abbreviations used:* AFMR, antiferromagnetic resonance; BWO, backward wave oscillator; EPR, electron paramagnetic resonance; FDMRS, frequency-domain magnetic resonance spectroscopy; HFEPR, high-frequency and -field EPR; HS, high-spin; LS, low-spin; *S*/*N*, signal-to-noise; zf, zero-field; zfs, zf splitting.

1090-7807/$ - see front matter © 2005 Elsevier Inc. All rights reserved.
doi:10.1016/j.jmr.2005.09.007

constructing a powder pattern, averaging over all spatial orientations of the single crystal with respect of the magnetic field. To assure the adequacy of fitted spin Hamiltonian parameters, HFEPR experiments have been often performed at multiple frequencies [10]; however, spin Hamiltonian parameters have usually been fitted to single-frequency spectra. More recently, spin Hamiltonian parameters have been fitted to a dataset containing a few discrete frequencies, usually obtained from the different harmonics of the Gunn oscillator source, which significantly improved the accuracy of spin Hamiltonian parameters obtained this way [11].

It was noticed early on that polycrystalline transition metal complexes spectra often do not display characteristics of powder patterns. The reason is the interaction of the crystallites with strong magnetic fields, which tends to align them with the direction of the largest magnetic susceptibility anisotropy parallel to the field. In certain cases the torquing effect is beneficial, resulting in quasi-single crystal spectra [12,13]. In most cases, however, the same effect is detrimental to spectral quality since it produces spectra that are neither ideally powder-patterned, nor single-crystal like, and renders them uninterpretable [14]. In addition, since single-mode cavity resonators are typically not used in HFEPR at frequencies above ~350 GHz, the microwave modes induced in oversized waveguides are not well defined and 'forbidden' transitions excited by B_1 parallel to B_0 are often observed with intensities comparable to the 'allowed' transitions, thus further complicating the powder patterns. We propose that the best way around the above-mentioned problems is an extension of the multifrequency HFEPR approach, which we call tunable-frequency HFEPR. This methodology dispenses with simulating single-frequency EPR spectra; instead, the frequency is tuned quasi-continuously, and resonances are plotted as a function of transition energy. This allows an easy visual recognition of particular spectral features. The optimal spin Hamiltonian parameters are subsequently best-fitted to the complete two-dimensional dataset of experimental resonances [15], the fitting procedure being now fully automated. This methodology has its roots in antiferromagnetic resonance (AFMR), where particular AFMR modes are also traced in the two-dimensional field-frequency space [16,17]. To achieve maximum frequency tunability, and consequently the maximum number of experimental points, we have taken advantage of backward wave oscillator (BWO) tubes as sub-THz wave radiation sources. BWOs have only rarely been employed in EPR in the past [18–20]. Shakurov and Tarasov [21] should be considered the inventors of their use in tunable-frequency EPR, as reflected in the title of their paper; however, their work did not involve high magnetic fields. The truly pioneering work was that of Alpert et al. [18], which combined the use of BWOs with high fields. In our application, four BWO tubes cover quasi-continuously the spectral range of 150–700 GHz (~5–23 cm^{-1}), although the range of BWOs in general is wider: ca. 24–1300 GHz (~1–43 cm^{-1}) [22].

In this article, we will show how tunable-frequency methodology using BWOs facilitates recognition of HFEPR spectral features, and improves the accuracy of spin Hamiltonian parameters obtained from imperfect powder spectra. While we have used tunable-frequency HFEPR in several recent papers devoted to specific problems in particular transition metal ions [3,23–25], the current work concentrates on, and discusses the advantages (and disadvantages) of this new magnetic resonance methodology. We will use as examples three non-Kramers ion complexes: Ni(II) ($3d^8$, $S = 1$) in a dichlorobistriphenylphosphane complex, $Ni(PPh_3)_2Cl_2$, where Ph = phenyl; Mn(III) ($3d^4$, $S = 2$) in mesotetrasulfonatoporphyrinatomanganese(III) chloride (hereafter abbreviated as Mn(TSP)Cl); Fe(II) ($3d^6$, $S = 2$) in ferrous sulfate tetrahydrate $Fe(SO_4)\cdot 4H_2O$; and one Kramers ion: HS Co(II) ($3d^7$, $S = 3/2$) in the complex azido(tris(3-*tert*-butylpyrazol-1-yl)hydroborate)cobalt(II) (hereafter abbreviated as $Tp^{tBu}CoN_3$); this ligand belongs to the trispyrazolylborate "scorpionate" family [26]. The Ni(II) and Mn(III) complexes have been studied before by HFEPR using the multifrequency methodology based on Gunn oscillator sources [9,27] but not the presently described tunable-frequency EPR. $Ni(PPh_3)_2Cl_2$ was also studied by Frequency-Domain Magnetic Resonance Spectroscopy (FDMRS) in zero, and low fields [28]. The $Fe(SO_4)\cdot 4H_2O$ and $Tp^{tBu}CoN_3$ complexes have not been hitherto studied by EPR to our best knowledge.

2. Results

2.1. $Ni(PPh_3)_2Cl_2$ ($3d^8$, $S = 1$)

A single-frequency (611 GHz) spectrum of polycrystalline $Ni(PPh_3)_2Cl_2$ is shown in Fig. 1 together with its simulation assuming an ideal powder pattern. It is clear that the experimental spectrum does not correspond to such a pattern. The B_{min} feature, which corresponds to an off-axis

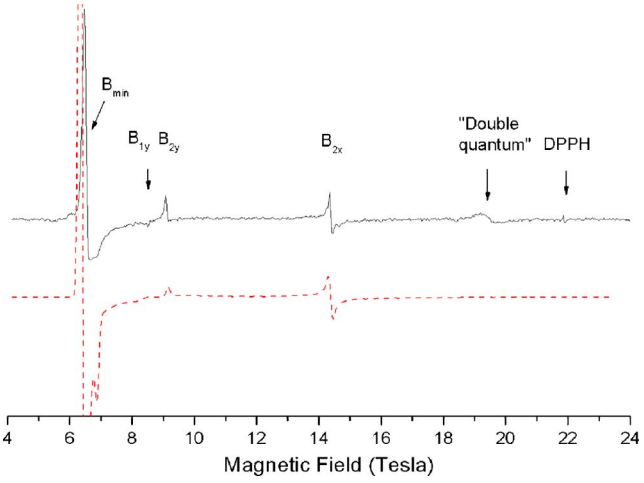

Fig. 1. Experimental (upper, solid) and simulated (lower, dashed) HFEPR spectra of $Ni(PPh_3)_2Cl_2$ at 611.2 GHz and 4.2 K. The parameters used in the simulation were those from Table 1.

turning point of the forbidden ($\Delta M_S = \pm 2$) transition, and is normally the strongest peak in a triplet powder spectrum [29], is at least one order of magnitude less intense than in the simulation. On the other hand, the B_{1y} turning point, which comes up in the simulation only if the oscillating field B_1 is assumed to have a component parallel to the Zeeman field B_0, distinctly appears in the experiment. Constraining the sample in a KBr-diluted pellet only minimally improves the picture [9], which is still very far from an ideal powder pattern. In this situation, obtaining moderately accurate values of the spin Hamiltonian parameters from the spectra was possible only through multi-frequency experiments using the multiple harmonics of the then available Gunn oscillator sources [9]. This study provided zfs parameters with an error of 0.05 cm^{-1} and anisotropy in the g-matrix could not be extracted, with an error in the resulting isotropic g value of 0.05. In the present work, we employed tunable-frequency HFEPR to collect and plot the resonances in polycrystalline $Ni(PPh_3)_2Cl_2$ as a function of sub-THz wave energy. Given the uncertainty of accurately locating the resonance position, we used the following rules: (a) for spectra that could be approximately simulated as powder patterns, we employed single-frequency simulations to determine the position of particular turning points; (b) for spectra that clearly originated from field-oriented samples, we compared them with simulated single-crystal spectra; (c) for intermediate cases we used our best judgment taking into account the shape of optically modulated spectra, which much better reflect the total shape of absorption than magnetically modulated ones. The field versus quantum energy dependence of resonances determined this way is shown in Fig. 2 as squares. This plot immediately offers several hints as to the origin of the observed turning points, and gives an estimate of spin Hamiltonian parameters. First, it was possible to directly detect two zero-field resonances at ca. 11.3 and 15 cm^{-1}, which are approximately the same values as those detected using FDMRS in a parallel study [28]. These were previously identified as $(D - E)$, and $(D + E)$ zero-field transitions. (For the actual shape of zfs resonances we refer to Fig. 1 in [9] in the case of magnetic modulation, and Fig. 5 in [3] in the case of optical modulation.) The third transition, $2E$, which should appear near 3.7 cm^{-1}, does not show up in the experiment since it occurs between the two excited spin sublevels of the triplet manifold, which are not significantly populated at low temperatures in case of positive D (see Chart 1). From Fig. 2 it is also easy to differentiate between the allowed ($\Delta M_S = \pm 1$) and forbidden ($\Delta M_S = \pm 2$) transitions, since the latter have a much less steep slope than the former, corresponding to a higher effective g value. The eventual identification of particular branches in the spectrum was achieved through simulations, which also finalized the spin Hamiltonian values as given in Table 1. Altogether, the fits yielded a remarkable agreement with the experiment, as witnessed by Fig. 2, and the small error values in spin Hamiltonian parameters as presented in Table 1. The values for D and E are in exact

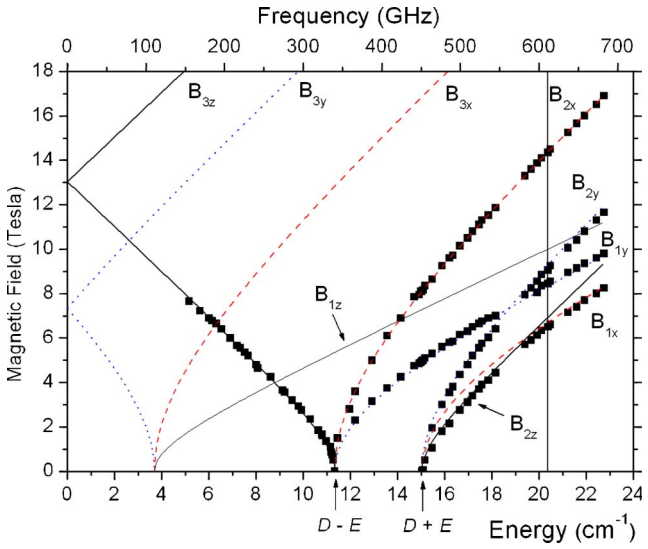

Fig. 2. Tunable-frequency HFEPR in an $S = 1$ spin system. Resonance field versus energy dependence of HFEPR resonances in $Ni(PPh_3)_2Cl_2$. Experimental resonance positions at specific frequencies are given by the squares. The lines were calculated using the best-fitted spin Hamiltonian parameters as in Table 1. Dashed lines: turning points with $B_0 \| x$; dotted lines: turning points with $B_0 \| y$, solid lines: turning points with $B_0 \| z$. The two zf transitions immediately recognizable at ca. 11.3 and 15 cm^{-1}, and the high-field calculated lines are identified using standard nomenclature for triplet states with rhombic symmetry [29] and labeled accordingly. The vertical line at 611.2 GHz (20.37 cm^{-1}) allows interpreting the single-frequency spectrum shown in Fig. 1.

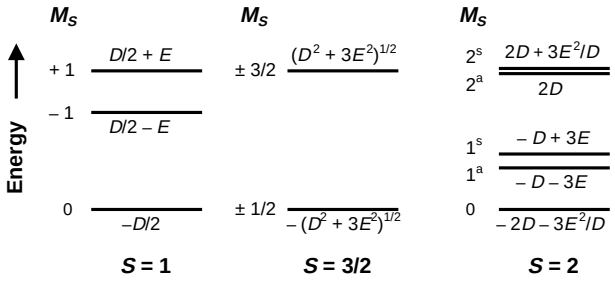

Chart 1. The result of second-rank zero-field splitting terms of spin Hamiltonian (1) in different spin multiplicities, for D and $E > 0$. We follow the terminology of Hendrich and Debrunner [43] to label spin levels of the quintet state and also note that the formulas for the $S = 2$ energies are derived using a perturbation approach, which makes them approximate.

agreement with those previously reported (see Table 1); however, the precision is now much higher: 0.002 cm^{-1} in D and 0.006 cm^{-1} in E, as opposed to 0.05 cm^{-1} obtained previously [9]. More significant is the ability, thanks to the combination of more numerous experimental points and automated fitting procedures, of determining g values with greater accuracy. The current value for g_x (2.200(5)) is the same as previously reported, but a significantly rhombic g-matrix, as expected from the rhombic zfs, is now apparent: $g_y = 2.177(1)$, $g_z = 2.15(1)$. The error in these values, particularly for g_x and g_y, is as much as 50 times smaller than in the previous study. As we have shown elsewhere [3], analysis of such an accurate g-matrix in an integer spin system can provide useful information on electronic structure

Table 1
Spin Hamiltonian parameters as determined by tunable-frequency EPR for the four HS complexes of studied in this work

Complex	S	D (cm^{-1})	E (cm^{-1})	g_x	g_y	g_z
$Ni(PPh_3)_2Cl_2$[a]	1	+13.196(2)	+1.848(6)	2.200(5)	2.177(1)	2.15(1)
$Tp^{tBu}CoN_3$	3/2	+7.457(2)	+1.575(3)	2.48(2)	2.02(1)	2.31(2)
Mn(TSP)Cl [b]	2	−3.116(6)	−0.0007(4)	1.996(1)	1.996(1)	2.01(1)
$Fe(SO_4)\cdot 4H_2O$	2	+10.32(1)	+2.23(1)	2.10(1)	2.04(1)	2.11(1)

[a] The following spin Hamiltonian parameters for $Ni(PPh_3)_2Cl_2$ were reported previously [9], based only on Gunn diode sources which provided relatively few frequencies: $D = +13.20(5)\ cm^{-1}$, $E = +1.85(5)\ cm^{-1}$, $g_{iso} = 2.20(5)$.
[b] Fourth-rank zfs parameters were also determined as follows: $B_4^0 = 9(4)$; $B_4^2 = 3(1)$; $B_4^4 = 19(7) \times 10^{-4}\ cm^{-1}$.

of the paramagnetic ion, although the zfs parameters are generally more informative in this respect.

2.2. $Tp^{tBu}CoN_3$ ($3d^7$, $S = 3/2$)

A single-frequency (377 GHz) spectrum of $Tp^{tBu}CoN_3$ is shown in Fig. 3 in both the optically and magnetically modulated versions (traces A and B, respectively) for a loose sample, and for a constrained sample (traces C and D), together with a simulation generated using spin Hamiltonian parameters as in Table 1 and assuming an ideal powder pattern (trace E). It is obvious that the experimental spectra do not correspond to such a pattern; in contrary, they suggest a strong alignment of the crystallites with field. An attempt to destroy this alignment by constraining the sample was only partially successful, although it causes some turning points to appear in the spectra that do not show up in the loose sample. The identification of the particular peaks in the $Tp^{tBu}CoN_3$ spectra was thus not possible based on single-frequency experiments, and neither was the determination of the spin Hamiltonian parameters from them. We therefore employed tunable-frequency HFEPR, and obtained a plot of all observed resonances in both the loose, and constrained sample, as a function of sub-THz quantum energy, shown in Fig. 4 as squares. The outstanding feature of this plot is the presence of a single zero-field transition near 480 GHz (16 cm^{-1}). This is the transition between the two Kramers manifolds: $\pm 1/2$, and $\pm 3/2$. Abbreviated as Δ, this energy value equals to $2|D|$ in the case of axial zfs, or $2(D^2 + 3E^2)^{1/2}$ for rhombic zfs [30,31]. It is thus possible to immediately estimate the magnitude of $|D|$ in $Tp^{tBu}CoN_3$ as ~8 cm^{-1}. The determination of the rhombic parameter E is, however, not possible for a Kramers spin system in zero field. The full set of spin Hamiltonian parameters including both zfs parameters D and E, and intrinsic values of the g-matrix, has been therefore obtained by a least-square fit to the complete two-dimensional array of resonances, as explained in Section 5. This fit resulted in the values as shown in Table 1. The quality of these parameters can be judged by the agreement of the calculated lines in Fig. 4 with the experimental resonances. The representation of HFEPR resonances as in Fig. 4 allows identifying particular resonance branches as

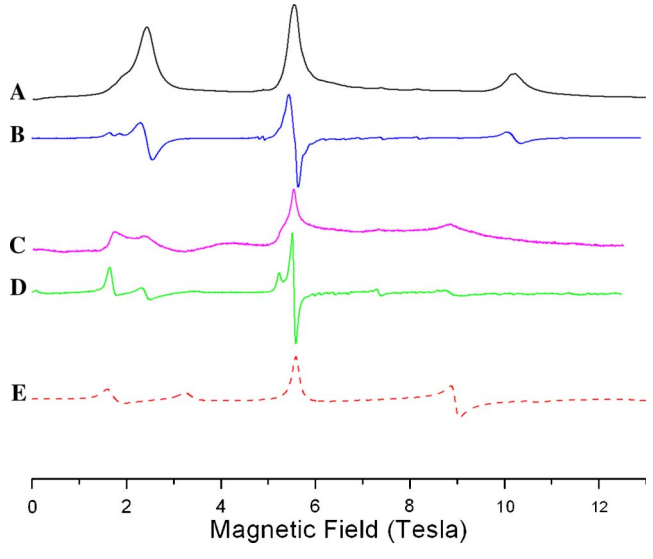

Fig. 3. HFEPR spectra of polycrystalline $Tp^{tBu}CoN_3$ at 377.4 GHz and 4.5 K. (A) Loose sample using optical modulation; (B) same spectrum as (A) in a derivative form using magnetic modulation; (C) constrained sample using optical modulation; (D) same spectrum as (C) in a derivative form using magnetic modulation; (E) derivative simulation assuming ideal powder pattern and using spin Hamiltonian parameters as in Table 1.

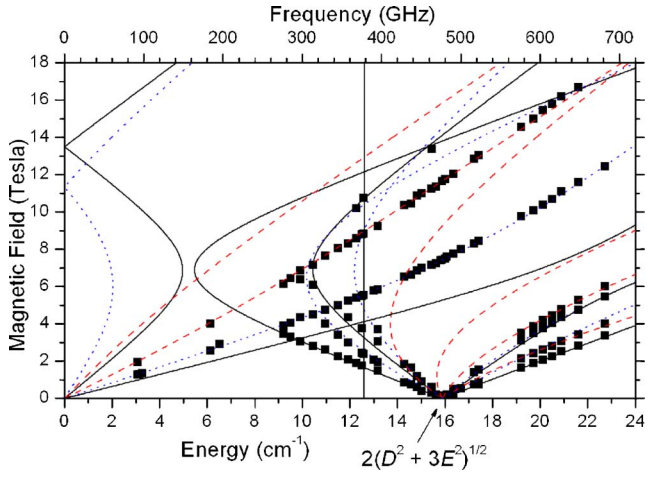

Fig. 4. Tunable-frequency HFEPR in an $S = 3/2$ spin system. Resonance field versus sub-THz quantum energy dependence for EPR transitions in $Tp^{tBu}CoN_3$. Experimental resonance positions at specific frequencies are given by the squares for both loose, and constrained sample. The lines were calculated using the best-fitted spin Hamiltonian parameters as in Table 1. Dashed lines: turning points with $B_0 \| x$; dotted lines: turning points with $B_0 \| y$, solid lines: turning points with $B_0 \| z$. The single zf transition at ~16 cm^{-1} characteristic for the quartet spin state is indicated by an arrow. The vertical line at 377.4 GHz (12.59 cm^{-1}) allows interpreting the single-frequency spectra shown in Fig. 3.

belonging to either the intra-Kramers ±1/2, or inter-Kramers transitions, i.e., between ±1/2 and ±3/2 manifolds. No intra-Kramers transitions within the ±3/2 manifold are detected at low temperatures [32]; on the other hand they show up at elevated temperatures (not shown), which proves that the ground Kramers doublet is the ±1/2 one, which corresponds to a positive sign of D.

Fig. 3 shows two kinds of spectra recorded for $Tp^{tBu}CoN_3$. Chopping the incident sub-THz beam results in spectra characterized by an absorptive shape. Such spectra give an immediate measure of the transition intensity, unlike the traditional, magnetically modulated spectra, which require numerical integration for the same purpose. We also show magnetically modulated spectra in the same conditions, together with their simulation, and defer the discussion of the respective merits of magnetic, and optical modulation until Section 3.

2.3. Mn(TSP)Cl ($3d^4$, $S = 2$, axial)

In contrast to the two HS complexes described above, $Ni(PPh_3)_2Cl_2$ and $Tp^{tBu}CoN_3$, and unlike most Mn(III) porphyrinic complexes, polycrystalline Mn(TSP)Cl does not torque in magnetic field, producing almost-perfect powder-patterned HFEPR spectra without any special sample preparation (Fig. 5, in both optically and magnetically modulations versions) [27]. In such a case it is possible to extract accurate spin-Hamiltonian parameters from single-frequency experiments, as was done before [27], and there is no pressing need for tunable-frequency HFEPR. However, not all Mn(III) complexes are as well-behaved as Mn(TSP)Cl; the majority of them undergo partial torquing in field with the consequence that spectra are quite often difficult to interpret [14]. We thus performed tunable-frequency HFEPR on polycrystalline Mn(TSP)Cl to illustrate the general usefulness of the method to $S = 2$ species in a case corresponding to an axial zfs tensor. The complete two-dimensional field-energy dataset for this quintet spin species is presented in Fig. 6 as squares. As was the case with the other high-spin systems studied, the experimental plots allow easy distinguishing between the allowed ($\Delta M_S = 1$), and the nominally forbidden ($\Delta M_S > 1$) transitions appearing in the spectra, the latter having a much less steep slope than the former. Also, one of the zero-field transitions was directly observed at about 9.3 cm^{-1}. This value may correspond to the $|D|$, $3|D|$, or $4|D|$ zf resonance in an axial spin quintet system. By analogy with other porphyrinic Mn(III) complexes we attribute it to the $3|D|$ zero-field resonance, which then immediately yields an estimate for $|D|$ of ~3.1 cm^{-1}. A rigorous least-square fit to the two-dimensional experimental dataset shown in Fig. 6 yields the spin Hamiltonian parameters as presented in Table 1. The fit results include fourth-order parameters as in Eq. (1b), which, although small, are different from zero. It should be mentioned that the quintet powder spectrum contains off-axis turning points in addition to canonical features. One such off-axis branch is visible in Fig. 6. Our program uses these experimental points as well, so that no single experimental resonance in the dataset is unaccounted for.

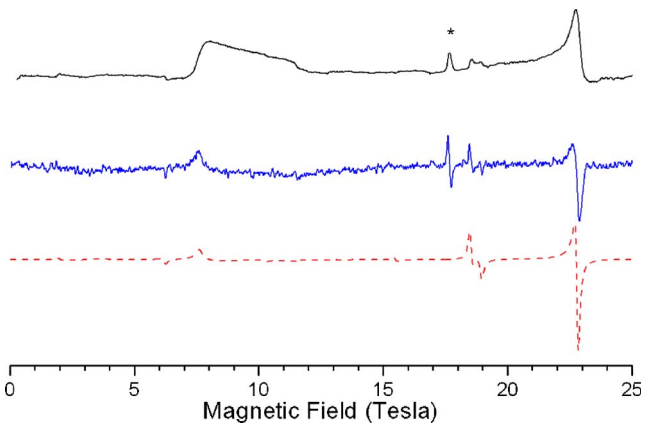

Fig. 5. Top trace: a 493.1 GHz spectrum of Mn(TSP)Cl at 8 K obtained using optical modulation; middle trace: the same spectrum in a derivative form using magnetic modulation; bottom (dashed) trace: a derivative simulation assuming a powder distribution and using spin Hamiltonian parameters as in Table 1. The peak marked with an asterisk originates from an Mn(II) impurity and is not reproduced in the simulation.

2.4. $Fe(SO_4)\cdot 4H_2O$ ($3d^6$, $S = 2$, rhombic)

A typical spectrum of $Fe(SO_4)\cdot 4H_2O$ pressed into a KBr pellet, recorded at 167 GHz is shown in Fig. 7 using both

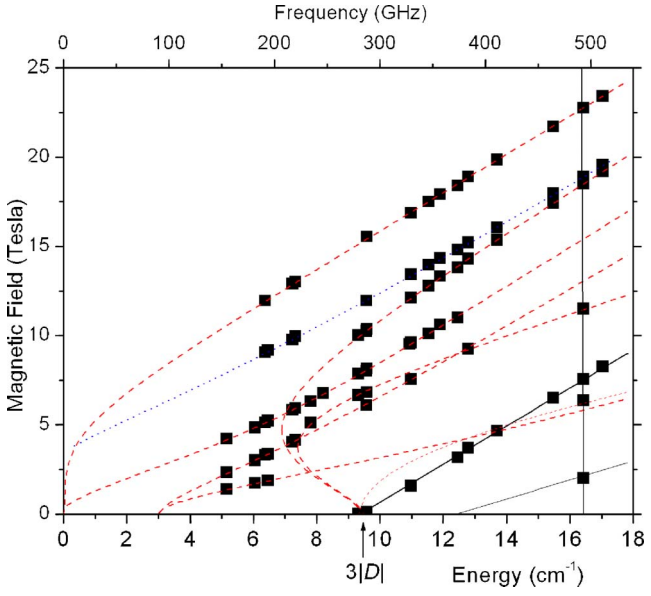

Fig. 6. Tunable-frequency HFEPR in an axial $S = 2$ spin system. Resonance field versus sub-THz quantum energy dependence for EPR transitions in Mn(TSP)Cl. Experimental resonance positions at specific frequencies are given by the squares. A single zf transition is directly detected at ca. 280 GHz (9.3 cm^{-1}) and indicated by an arrow. The lines were calculated using the best-fitted spin Hamiltonian parameters as in Table 1 and are shown by a solid line for parallel turning points, dashed lines for perpendicular turning points, and a dotted line for the off-axis turning points. For clarity, only those branches of turning points are simulated that were experimentally observed. The vertical line at 493.1 GHz (16.44 cm^{-1}) allows interpreting the single-frequency spectra shown in Fig. 5.

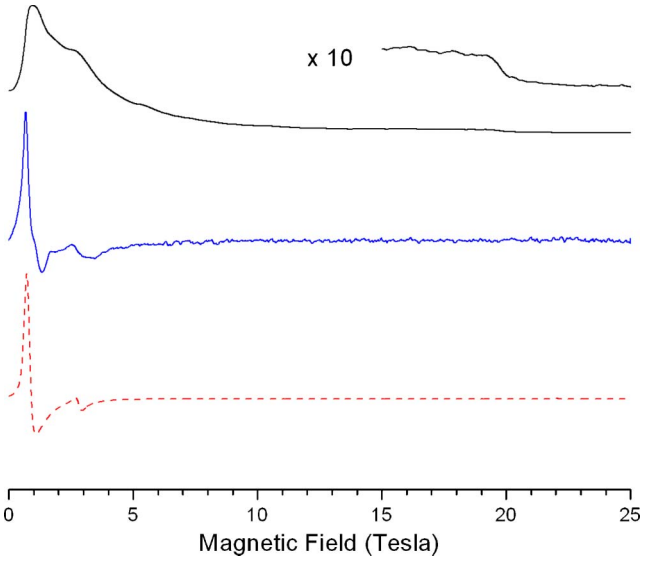

Fig. 7. (Top trace) Optically modulated HFEPR spectrum of $Fe(SO_4)\cdot 4H_2O$ pressed into a KBr pellet at 167 GHz and 4.5 K (with the high-field part of the spectrum magnified 10× to better show a turning point at 19.5 T); (middle trace) a derivative-shaped magnetically modulated spectrum of the same sample in identical conditions; (bottom (dashed) trace) a derivative simulation assuming powder distribution and using parameters optimized for this particular frequency: $D = 10.5$, $E = 2.4\ \mathrm{cm}^{-1}$, g values as in Table 1.

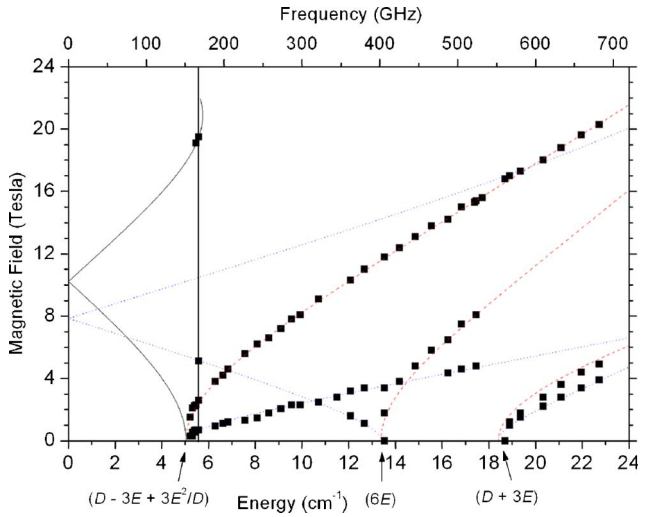

Fig. 8. Tunable-frequency HFEPR in a rhombic $S = 2$ spin system. Resonance field versus sub-THz quantum energy dependence for EPR transitions in $Fe(SO_4)\cdot 4H_2O$ (both loose and constrained sample). The squares are experimental points while the lines were simulated using best-fitted spin Hamiltonian parameters given in Table 1. Dashed lines: turning points with $B_0 \| x$; dotted lines: turning points with $B_0 \| y$, solid line: turning points with $B_0 \| z$. For clarity, only those branches of turning points were simulated that were experimentally observed. The vertical line at 167 GHz ($5.57\ \mathrm{cm}^{-1}$) allows interpreting the single-frequency spectra shown in Fig. 7. Note the turning point at 19.5 T that appears in the optically modulated spectrum in Fig. 7, but does not come up in the magnetically modulated spectra.

optical and magnetic modulation. Although single-frequency spectra could be in some cases reasonably well simulated assuming powder distribution, as shown in Fig. 7, these spectra are also poor in recognizable features, and as such, could not be immediately interpreted before collecting a full field versus energy data set.

A full field versus energy dependence of EPR resonances observed in $Fe(SO_4)\cdot 4H_2O$ in both loose, and constrained samples, is presented as squares in Fig. 8. The prominent feature of this plot is the presence of three zf resonances, appearing at ca. 5, 13.5, and $18.5\ \mathrm{cm}^{-1}$. Since the low-frequency value ($5\ \mathrm{cm}^{-1}$) is approximately the difference of the two high frequencies (13.5 and $18.5\ \mathrm{cm}^{-1}$), a possible initial assignment of the zf resonances is to attribute them to the $6E$, $(D - 3E)$, and $(D + 3E)$ zf transitions, respectively (ignoring the $3E^2/D$ factor in the case of low rhombicity). This assignment results in the following, largely axial, values of the zfs parameters: $D = 16$; $E = 0.83\ \mathrm{cm}^{-1}$. However, an attempt to fit the field versus energy resonances dependencies using these parameters was wholly unsuccessful. Instead, the following assignment of the three observed zf resonances: $(D - 3E + 3E^2/D)$, $(6E)$, $(D + 3E)$ results in the values: $D = 10.5$, $E = 2.25\ \mathrm{cm}^{-1}$ and an immediate agreement between the simulation and experiment (Fig. 8). A computer fit refined the values of the zfs parameters, and provided the g-matrix values. The final spin Hamiltonian parameters are thus: $D = +10.32(1)\ \mathrm{cm}^{-1}$, $E = +2.23(1)\ \mathrm{cm}^{-1}$, $g_x = 2.10(1)$, $g_y = 2.04(1)$, $g_z = 2.11(1)$.

3. Discussion

3.1. Tunable-frequency HFEPR of non-Kramers and Kramers metal ions

The origin of the zero-field splitting (zfs), which is the splitting of the M_S levels corresponding to the ground spin state, lies in the admixture of higher-lying excited states to the ground state [33]. As the name implies, this phenomenon happens in the absence of magnetic field, and the zfs constants as they appear in Hamiltonian (1) are field-independent. The excited-states admixture is mediated through the spin–orbit coupling, which can strongly vary from one system to another. This, plus different magnitudes of the ligand-field splitting and the symmetry considerations, cause high-spin transition metal complexes to display a stunning variety of zfs magnitude, from very small, on the order of $10^{-2}\ \mathrm{cm}^{-1}$ (e.g., Mn(II) in high-symmetry environments) to $10^2\ \mathrm{cm}^{-1}$ (e.g., Co(II) in octahedral symmetry). If we ignore the extreme cases, the range of $1–40\ \mathrm{cm}^{-1}$ is quite typical for high-spin transition metal ions. The use of tunable radiation sources operating in the sub-THz regime in combination with high magnetic fields in the 0–25 T range assures that many if not most transitions between spin sublevels in these systems are spectrally covered. This is particularly important for non-Kramers metal ions, where the zero-field degeneracy within the particular $\pm M_S$ manifolds is lifted in zero-field conditions in the case of low symmetry

[20]. We have shown above how tunable-frequency EPR is able to accurately deliver spin Hamiltonian parameters for three important non-Kramers transition metal ions, Ni(II), Mn(III), and Fe(II), which are typically 'EPR-silent' at conventional frequencies and fields. The accuracy of measurements is particularly worth stressing since previously most, if not all, information on the spin Hamiltonian parameters of these, and similar systems came from non-resonant techniques such as magnetic susceptibility measurements [2], which only rarely yielded accurate values.

The Kramers spin species differ from non-Kramers systems in that there is always at least one allowed ($\Delta M_S = \pm 1$) transition at any frequency independent of the zfs magnitude, as follows from Chart 1. Consequently, a Kramers ion is, at least in principle, never 'EPR-silent' at conventional frequencies or fields. However, zfs does influence the EPR properties of such species while it cannot usually be determined directly or accurately. This has traditionally necessitated the use of the 'effective spin' concept, in which the magnetic properties of the given HS Kramers species are described in terms of fictitious low spin $S' = 1/2$ and a corresponding spin Hamiltonian. We have shown above how HFEPR in its tunable version allows one to discard the 'effective spin' methodology for HS Co(II), and determine not only accurate values of its zfs parameters, but also intrinsic values of the g-matrix, as opposed to the 'effective spin' concept.

The accuracy in spin Hamiltonian parameters obtained in this work comes at a cost of acquiring a relatively large number of spectra, each at a different frequency. Of particular importance in this respect is our use of an EPR-quality resistive magnet. Thanks to the high sweep rate of such a magnet (typically 5 T/min), the number of spectra acquired within a given time unit is one order of magnitude higher than that obtained in superconducting magnets, more often used in HFEPR. On the other hand, the sweep rate is much lower than that characteristic for pulsed magnets, making conventional detection schemes applicable.

In principle, it should be possible to observe EPR resonances in any HS system if the single operating frequency is higher than the magnitude of zfs splitting, or available magnetic field brings the respective M_S levels close enough to afford detection. While this is certainly true, there are several instances, presented above, where the spectra do not correspond to ideal powder patterns thus making the recognition of spectral features difficult or impossible. The application of tunable frequency greatly facilitates the recognition of these features. Most importantly, it offers a unique opportunity to tune in to zero-field resonances, thus measuring directly the zfs parameters in the absence of field. Applying (high) magnetic fields subsequently verifies the attribution of zf resonances in complicated spin systems (such as the quintet, or higher-multiplicity states), allows refinement of the zfs parameters, and serves to accurately establish the g-matrix values, thus completing the process of extracting a complete spin Hamiltonian parameter set.

3.2. Sensitivity considerations

Tunable-frequency EPR is not free of disadvantages, compared to single-frequency experiments. One of the most important is a relatively moderate sensitivity [27,34] compared to single-frequency spectrometers, which are optimized to perform at a specific frequency. The optimization usually involves applying a single-mode resonator, which significantly increases the B_1 field incident on the sample. In contrast, a tunable-frequency instrument needs to have a broadband response, which usually comes at the expense of sensitivity. An interesting effort at a "best-of-both-worlds" methodology was recently developed by Hill and co-workers [35]. Their method uses relatively broadly tunable Gunn sources in conjunction with an oversized resonator. As such this methodology combines the advantages of a cavity with those of tunable-frequency method, but so far it has been employed only at frequencies below ca. 350 GHz.

The limited sensitivity of broadly tunable EPR has a negative impact on investigating samples with low spin concentrations, notably metalloproteins. Nevertheless tunable-frequency EPR, as shown in this work, is perfectly suited for measuring simple coordination complexes, some of which serve as models for the more complicated biomolecules, whether in polycrystalline form, or in moderately concentrated solutions. Also, because the instruments employing no resonators can accept large amounts of polycrystalline sample, or frozen solution, the concentration sensitivity of such an experiment (as opposed to absolute sensitivity) needs not be significantly lower than that in resonator-equipped spectrometers, as discussed by some of us in [27].

3.3. Optical versus magnetic modulation

Given that the sub-THz wave beam in our apparatus partly propagates through free space, we used an optical chopper to modulate the beam for detection purposes in some experiments. The resulting spectra (Figs. 3, 5 and 7) give a direct measure of the sample's transmission (or absorption) at a given field. As such, they are equivalent to the standard, magnetically modulated EPR spectra that have been numerically integrated. Optical modulation has at least two advantages over the magnetic one: (a) for broad lines, as normally observed in magnetically non-diluted transition metal complexes, it typically offers a much better S/N ratio than the magnetic modulation (see [36], Chapter 6F,) and (b) it is less prone to fast-passage effects as often observed in the same complexes at low temperatures and high magnetic fields. The former advantage is nicely illustrated in Fig. 7: while the optical modulation succeeds in detecting a perpendicular turning point at 5.1 T and its parallel equivalent at 19.5 T at 167 GHz, the magnetic modulation completely misses both of them. The same turning points are so weak in an ideal magnetically modulated powder pattern as simulated in the bottom

trace of Fig. 7 that showing them would require magnifying the plot by a factor of 100 and reducing their linewidths to unreasonable values. Optical modulation is also quite instructive in showing the reason for the intrinsically limited sensitivity of HFEPR of HS transition metal ions such as those presented in this study, independent of the experimental setup. Fig. 5 shows that the EPR absorption in the ground $\langle S,\ M_S| = \langle\ 2,\ -2|$ spin state in the Mn(TSP)Cl polycrystalline complex covers the field range of more than 16 T, at high enough frequency. Magnetic modulation detects only the two turning points of this absorption, at ca. 7.5 and 23 T, which are normally quite broad, and this results in a relatively low S/N ratio. The excited spin states such as $\langle\ 2,\ -1|$ contribute at elevated temperatures (the small absorption between 18 and 19 T in Fig. 5), but in this regime the spin-lattice relaxation causes a general decline of S/N. In this example, the zfs is comparatively small ($|D| \sim 3\ \mathrm{cm}^{-1}$). For larger magnitude zfs, it would be impossible to cover the complete absorption envelope even with the high frequencies and fields currently available.

Among the drawbacks of the optical modulation relative to its magnetic version is the high sensitivity to any kind of instabilities in the system, particularly of the thermal nature. These normally result in a baseline shift and can seriously distort the spectra. Also, the mechanical beam modulation implies low modulation frequencies, which are usually far from optimal because of the $1/f$ source noise.

4. Conclusions

We present a novel version of high-field electron paramagnetic resonance, which we term tunable-frequency HFEPR. This methodology depends on the use of tunable sub-THz radiation sources (backward wave oscillators) in conjunction with an EPR-quality resistive magnet, and proves particularly useful in determining very accurate spin Hamiltonian parameters for high-spin transition metal ions in low-symmetry environment characterized by large zero-field splitting. As examples, we show applications to polycrystalline samples of three different non-Kramers (integer-spin number) species: Mn(III) (d^4, $S = 2$), Fe(II) (d^6, $S = 2$), and Ni(II) (d^8, $S = 1$), which are usually 'EPR-silent' in conventional conditions, and one Kramers (half-integer number) ion: Co(II) (d^7, $S = 3/2$), which, although 'EPR-active' at low frequencies, typically remains uninformative in these conditions.

5. Experimental

5.1. Samples

$Ni(PPh_3)_2Cl_2$ was purchased from Sigma–Aldrich, Mn(TSP)Cl from Porphyrin Products, and $Fe(SO_4)\cdot 4H_2O$ from Fisher Scientific, the latter sample in a form of a heptahydrate. Ferrous sulfate heptahydrate was allowed to sit at room temperature for prolonged time. Like all other samples, it was also pumped on during experiment preparation. It is known that under these conditions ferrous heptahydrate converts to tetrahydrate by releasing some of the coordinated water molecules [37]. $Tp^{tBu}CoN_3$ was synthesized as described previously [38]. All HFEPR experiments were performed on ca. 20–40 mg of loose polycrystalline samples, some of which were ground in an agate mortar prior to experiment. The torquing effects in high magnetic fields necessitated pressing KBr-diluted pellets in the case of the $Fe(SO_4)\cdot 4H_2O$. Other details of sample preparation are described in the referenced papers.

5.2. HFEPR spectroscopy

HFEPR spectra were recorded using the mm and Submm Wave Spectroscopy Facility at NHMFL [39]. Tunable frequencies in the 150–700 GHz range (~5–23 cm^{-1}) were provided by a set of four BWOs (purchased from the Institute of General Physics, Moscow, Russian Federation). The high-voltage power supply and the permanent magnet housing for the tubes were acquired from the same source. The frequency was pre-calibrated using a Fabry–Pèrot resonator. The magnet used was the resistive "Keck" magnet (0–25 T) of improved homogeneity (12 ppm in 1 cm diameter spherical volume) and temporal stability. The field was pre-calibrated using an NMR probe, and checked during the experiment using a DPPH marker. The oversized-pipe wave propagation system was home-built along the principles outlined before [34]. No resonator was employed. Detection was provided with an InSb hot-electron bolometer (QMC, Cardiff, UK). Modulation for detection purposes was provided alternatively by modulating the magnetic field (typically 1 kHz frequency, 2 mT maximum amplitude), or by chopping the sub-THz wave beam at ca. 300 Hz. A Stanford SR830 lock-in amplifier converted the modulated signal to DC voltage.

5.3. EPR analysis

The magnetic properties of a high-spin species can be described by the standard spin Hamiltonian composed of Zeeman and zfs terms [2]:

$$\mathscr{H} = \beta B \cdot g \cdot S + D(S_z^2 - S(S+1)/3) + E(S_x^2 - S_y^2) \qquad (1a)$$

for $S \leqslant 3/2$ spin species, or

$$\mathscr{H} = \beta B \cdot g \cdot S + D(S_z^2 - S(S+1)/3) + E(S_x^2 - S_y^2) + B_4^0 O_4^0 + B_4^2 O_4^2 + B_4^4 O_4^4 \qquad (1b)$$

for higher spin numbers. Because undiluted solid-state samples are characterized by strong spin–spin interactions, hyperfine structure is generally not observed in such conditions. We have thus ignored the hyperfine terms of the Hamiltonian. Higher-order Zeeman terms were neglected, too. The results of the zero-field terms of spin Hamiltonian (1a) acting on the spin wavefunctions of the triplet, quartet, and quintet states are shown in Chart 1. The transitions

between all the spin energy levels are equally probable in zero field.

The spin Hamiltonian parameters were extracted from the HFEPR spectra in the following way. The initial parameters D and E were estimated from zero-field resonances. Subsequently, assuming reasonable g-matrix elements, all transitions observed in experimental spectra were identified as corresponding to the $B\|x$, y, z, or to the off-axial orientations. A two-dimensional array whose rows contained frequency, Θ, Φ, and resonance field, collected from all single-frequency spectra, was used as input data. A computer program minimized the function

$$\chi^2 = \sum_{i=1}^{N} (f_i^{(\mathrm{calc})} - f_i^{(\mathrm{exp})})^2$$

by use of the Simplex method. Because we assumed (and confirmed in separate experiments described in [34]) that all experimental resonance fields bear approximately the same uncertainty, there was no need to include uncertainties χ_i^2 in the denominator. The resonance fields, $f_i^{(\mathrm{calc})}$ were calculated using the well-known formulas resulting from the exact solution of the secular equation [29] for the triplet ($S = 1$) state. The $S = 3/2$ and $S = 2$ resonance fields were calculated in an iterative procedure that employed the Householder method [40] to diagonalize the spin Hamiltonian in Eqs. 1a and 1b. After convergence had been achieved, the Hessian matrix was calculated [41] from

$$H_{ij} = \sum_{k=1}^{N} \left(\frac{\delta f_k^{calc}}{\delta p_i}\right)\left(\frac{\delta f_k^{calc}}{\delta p_j}\right)$$

The derivatives of the resonance fields, f_k^{calc}, with respect to the parameters p had to be evaluated numerically. Errors in the best-fit parameters were finally estimated as

$$\sigma_i = \sqrt{\frac{\chi^2}{N-P}(H^{-1})_{ii}},$$

where N is the number of experimental resonance fields and P is the number of fitted parameters.

In single-frequency spectral simulations transition probabilities of the transitions excited by B_1 perpendicular to B_0 were calculated from the eigenvectors in a standard way [42], and the calculated transition intensities were corrected for the Boltzmann populations of the levels involved. Transition probabilities for the case of B_1 parallel to B_0 were calculated as well. Finally, a powder pattern averaging all orientations in space was created. In all simulations we assumed a co-linearity of the $\boldsymbol{g}$- and zfs tensors. All the software used in the calculations presented in this work was locally written.

Acknowledgments

We thank Dr. Boris Gorshunov from the Institute of General Physics, Moscow, for bringing to our attention the qualities of BWOs as potential tunable-frequency sources for HFEPR. The late Dr. Jack Crow, and Dr. Bruce Brandt from NHMFL are acknowledged for their active support of this project. NHMFL is funded by the National Science Foundation through Cooperative Agreement DMR 0084173, and the State of Florida. The W.M. Keck Foundation funded the high-homogeneity resistive magnet.

References

[1] G.M. Smith, P.C. Riedi, in: B.C. Gilbert, M.J. Davies, D.M. Murphy (Eds.), Electron Paramagnetic Resonance, Royal Society of Chemistry, Cambridge, UK, 2002, pp. 254–303.
[2] A. Abragam, B. Bleaney, Electron Paramagnetic Resonance of Transition Ions, Dover, New York, 1986.
[3] J. Krzystek, A.T. Fiedler, J.J. Sokol, A. Ozarowski, S.A. Zvyagin, T.C. Brunold, J.R. Long, L.-C. Brunel, J. Telser, Pseudo-octahedral complexes of vanadium(III): electronic structure investigation by magnetic and electronic spectroscopy, Inorg. Chem. 43 (2004) 5645–5658.
[4] A.-L. Barra, D. Gatteschi, R. Sessoli, G.L. Abbati, A. Cornia, A.C. Fabretti, M.G. Uytterhoeven, Electronic structure of manganese(III) compounds from high-frequency EPR spectra, Angew. Chem. Int. Ed. 36 (1997) 2329–2331.
[5] J. Krzystek, J. Telser, L.A. Pardi, D.P. Goldberg, B.M. Hoffman, L.-C. Brunel, High-frequency and -field electron paramagnetic resonance of high-spin manganese(III) in porphyrinic complexes, Inorg. Chem. 38 (1999) 6121–6129.
[6] J. Telser, L.A. Pardi, J. Krzystek, L.-C. Brunel, EPR spectra from 'EPR-silent' species: high-field EPR spectroscopy of aqueous chromium(II), Inorg. Chem. 37 (1998) 5769–5775.
[7] M.J. Knapp, J. Krzystek, L.-C. Brunel, D.N. Hendrickson, High-frequency EPR study of the ferrous ion in the reduced rubredoxin model $[Fe(SPh)_4]^{2-}$, Inorg. Chem. 39 (2000) 281–288.
[8] L.A. Pardi, A.K. Hassan, F.B. Hulsbergen, J. Reedijk, A.L. Spek, L.-C. Brunel, Direct determination of the single-ion anisotropy in a one-dimensional magnetic system by high-field EPR spectroscopy; synthesis, EPR, and X-ray structure of $Ni_xZn_{1-x}(C_2O_4)(dmiz)_2$ [$x = 0.07$], Inorg. Chem. 39 (2000) 159–164.
[9] J. Krzystek, J.-H. Park, M.W. Meisel, M.A. Hitchman, H. Stratemeier, L.-C. Brunel, J. Telser, EPR spectra from "EPR-silent" species: high-frequency and -field EPR spectroscopy of pseudo-tetrahedral complexes of nickel(II), Inorg. Chem. 41 (2002) 4478–4487.
[10] P.J.M. van Kan, E. van der Horst, E.J. Reijerse, P.J.M. van Bentum, W.R. Hagen, Multi-frequency EPR spectroscopy of myoglobin. Spectral effects for high-spin iron(III) ion at high magnetic fields, J. Chem. Soc. Faraday Trans. 94 (1998) 2975–2978.
[11] P.L.W. Tregenna-Piggott, H. Weihe, A.-L. Barra, High-field, multi-frequency EPR study of the $[Mn(OH_2)_6]^{3+}$ cation: influence of π-bonding on the ground state zero-field-splitting parameters, Inorg. Chem. 42 (2003) 8504–8508.
[12] A.L. Barra, A. Caneschi, D. Gatteschi, R. Sessoli, High-frequency EPR spectra for the analysis of magnetic anisotropy in large magnetic clusters, J. Am. Chem. Soc. 117 (1995) 8855–8856.
[13] D.P. Goldberg, J. Telser, J. Krzystek, A.G. Montalban, L.-C. Brunel, A.G.M. Barrett, B.M. Hoffman, EPR spectra from "EPR-silent" species: high-field EPR spectroscopy of manganese(III) porphyrins, J. Am. Chem. Soc. 119 (1997) 8722–8723.
[14] J. Krzystek, G. Yeagle, J.-H. Park, M.W. Meisel, R.D. Britt, L.-C. Brunel, J. Telser, High frequency and field EPR spectroscopy of tris(2,4-pentanedionato)manganese(III): investigation of solid-state versus solution Jahn–Teller effects, Inorg. Chem. 42 (2003) 4610–4618.
[15] L.A. Pardi, J. Krzystek, J. Telser, L.-C. Brunel, Multifrequency EPR spectra of molecular oxygen in solid air, J. Magn. Reson. 146 (2000) 375–378.

[16] G.E. Fanucci, J. Krzystek, M.W. Meisel, L.-C. Brunel, D.R. Talham, Antiferromagnetic resonance as a tool for investigating magneto-structural correlations: the canted antiferromagnetic state of $KMnPO_4{\cdot}H_2O$ and a series of manganese phosphonates, J. Am. Chem. Soc. 120 (1998) 5469–5479.
[17] K. Katsumata, High-frequency electron spin resonance in magnetic systems, J. Phys. Condens. Matter 12 (2000) R589–R614.
[18] Y. Alpert, J. Couder, J. Tuchendler, H. Thome, Determination of the zero-field splitting in human acid methemoglobin by millimeter and submillimeter ESR experiments, Biochim. Biophys. Acta 332 (1973) 34–37.
[19] A.G. Anders, S.V. Volotskiy, V.V. Eremenko, S.A. Zvyagin, V.A. Novosad, V.V. Pishko, Magnetodipole excitations and ground state of the rare-earth ion in Sm_2CuO_4, Low Temp. Physics 10 (1993) 814.
[20] V.F. Tarasov, G.S. Shakurov, B.Z. Malkin, V.A. Ulanov, Submillimeter EPR of non-Kramers ions, in: C.Z. Rudowicz (Ed.), Modern Applications of EPR/ESR, Springer, Singapore, 1998.
[21] G.S. Shakurov, V.F. Tarasov, High-frequency tunable EPR spectroscopy of Cr^{3+} in synthetic forsterite, Appl. Magn. Reson. 21 (2001) 597–605.
[22] G. Kozlov, A. Volkov, Coherent source submillimeter wave spectroscopy, in: G. Gruner (Ed.), Millimeter and Submillimeter Wave Spectroscopy of Solids, Topics in Applied Physics, vol. 74, Springer, Berlin, 1998.
[23] S.A. Zvyagin, A.K. Kolezhuk, J. Krzystek, R. Feyerherm, Excitation hierarchy of the quantum sine-Gordon spin chain in a strong magnetic field, Phys. Rev. Lett. 93 (2004) 027201.
[24] A. Ozarowski, S.A. Zvyagin, W.M. Reiff, J. Telser, L.C. Brunel, J. Krzystek, High-frequency and -field EPR of a pseudo-octahedral complex of high-spin Fe(II): bis(2,2′-bi-2-thiazoline)bis(isothiocyanato)iron(II), J. Am. Chem. Soc. 126 (2004) 6574–6575.
[25] J. Krzystek, S.A. Zvyagin, A. Ozarowski, A.T. Fiedler, T.C. Brunold, J. Telser, Definitive spectroscopic determination of zero-field splitting in high-spin cobalt(II), J. Am. Chem. Soc. 126 (2004) 2148–2155.
[26] S. Trofimenko, Scorpionates: The Coordination Chemistry of Polypyrazolylborate Ligands, Imperial College Press, London, UK, 1999.
[27] J. Krzystek, J. Telser, High frequency and field EPR spectroscopy of Mn(III) complexes in frozen solutions, J. Magn. Reson. 162 (2003) 454–465.
[28] S. Vongtragool, B. Gorshunov, M. Dressel, J. Krzystek, D.M. Eichhorn, J. Telser, Direct observation of fine structure transitions in a paramagnetic nickel(II) complex using far-infrared magnetic spectroscopy: a new method for studying high-spin transition metal complexes, Inorg. Chem. 42 (2003) 1788–1790.
[29] P. Kottis, R. Lefebvre, Calculation of the electron spin resonance (E.S.R.) line shape of randomly oriented molecules in a triplet state. II. Correlation of the spectrum with the zero-field splittings. Introduction of an orientation-dependent line width, J. Chem. Phys. 41 (1964) 379–393.
[30] M.W. Makinen, L.C. Kuo, M.B. Yim, G.B. Wells, J.M. Fukuyama, J.E. Kim, Ground term splitting of high-spin Co^{2+} as a probe of coordination structure. 1. Dependence of the splitting on coordination geometry, J. Am. Chem. Soc. 107 (1985) 5245–5255.
[31] J.A. Larrabee, C.M. Alessi, E.T. Asiedu, J.O. Cook, K.R. Hoerning, L.J. Klingler, G.S. Okin, S.G. Santee, T.L. Volkert, Magnetic circular dichroism spectroscopy as a probe of geometric and electronic structure of cobalt(II)-substituted proteins: ground-state zero-field splitting as a coordination number indicator, J. Am. Chem. Soc. 119 (1997) 4182–4196.
[32] Although nominally forbidden, these transitions do show up at certain conditions.
[33] R. Boca, Zero-field splitting in metal complexes, Coord. Chem. Rev. 248 (2004) 757–815.
[34] A.K. Hassan, L.A. Pardi, J. Krzystek, A. Sienkiewicz, P. Goy, M. Rohrer, L.-C. Brunel, Ultrawide band multifrequency high-field EMR technique: a methodology for increasing spectroscopic information, J. Magn. Reson. 142 (2000) 300–312.
[35] E.-C. Yang, C. Kirman, J. Lawrence, L.N. Zakharov, A.L. Rheingold, S. Hill, D.N. Hendrickson, Single-molecule magnets: high-field electron paramagnetic resonance evaluation of the single-ion zero-field interaction in a $Zn^{II}_3Ni^{II}$ complex, Inorg. Chem. 44 (2005) 3827–3836.
[36] C.P. Poole, Electron Spin Resonance, Dover, Mineola, 1983.
[37] A.G. Mitchell, The preparation and characterization of ferrous sulfate hydrates, Can. J. Pharm. Pharmacol. 36 (1984) 506–510.
[38] S. Trofimenko, J.C. Calabrese, J.S. Thompson, Novel polypyrazoylborate ligands: coordination control through 3-substituents of the pyrazol ring, Inorg. Chem. 26 (1987) 1507–1514.
[39] S.A. Zvyagin, J. Krzystek, P.H.M. van Loosdrecht, G. Dhalenne, A. Revcolevschi, High-field ESR study of the dimerized-incommensurate phase transition in the spin-Peierls compound $CuGeO_3$, Physica B 346–347 (2004) 1–5.
[40] J.H. Wilkinson, The Algebraic Eigenvalue Problem, Clarendon Press, London, 1970.
[41] W.H. Press, B.P. Flannery, A.A. Teukolsky, W.T. Vetterling, Numerical Recipes in Pascal, Cambridge University Press, Cambridge, 1989, p. 572.
[42] A. Bencini, D. Gatteschi, ESR spectra of metal complexes of the first transition series in low- symmetry environments, in: G.A. Melson, B.N. Figgis (Eds.), Transition Metal Chemistry, vol. 8, Marcel Dekker, New York, 1982.
[43] M.P. Hendrich, P.G. Debrunner, Integer-spin electron paramagnetic resonance of iron proteins, Biophys. J. 56 (1989) 489–506.